Surface albedo darkening from wildfires in northern sub-Saharan Africa

C K Gatebe[1,2]**, C M Ichoku**[2]**, R Poudyal**[1,3]**, M O Román**[2] **and E Wilcox**[4]

[1] Universities Space Research Association, Columbia, Maryland 20146, USA
[2] NASA Goddard Space Flight Center, Greenbelt, Maryland 20771, USA
[3] Science Systems and Applications, Inc, Lanham, Maryland, USA
[4] Desert Research Institute, Reno, Nevada 89512, USA

E-mail: charles.k.gatebe@nasa.gov

Abstract

Northern sub-Saharan Africa (NSSA) has a wide variety of climate zones or biomes, where albedo dynamics are highly coupled with vegetation dynamics and fire disturbances. Quantifying surface albedo variations due to fire disturbances on time scales of several months to several years is complex and is made worse by lack of accurate and spatially consistent surface albedo data. Here, we estimate the surface albedo effect from wildfires in different land cover types in the NSSA region using Moderate Resolution Imaging Spectroradiometer (MODIS) multi-year observational data (2003–11). The average decrease in albedo after fires at the scale of 1 km MODIS footprint is $-0.002\,02 \pm 0.000\,03$ for woody savanna and $-0.002\,22 \pm 0.000\,03$ for savanna. These two land cover types together account for >86% of the total MODIS fire count between 2003 and 2011. We found that only a small fraction of the pixels ($\leqslant$10%) burn in two successive years and about 47% had any fire recurrence in 9 years. The study also derived the trajectories of post-fire albedo dynamics from the percentages of pixels that recover to pre-fire albedo values each year. We found that the persistence of surface albedo darkening in most land cover types in the NSSA region is limited to about 6–7 years, after which at least 99% of the burnt pixels recover to their pre-fire albedo. Our results provide critical information for deriving necessary input to various models used in determining the effects of albedo change due to wild fires in the NSSA region.

Keywords: surface albedo, wildfires, sub-Saharan Africa, MODIS, biomass burning, albedo recovery, albedo darkening

1. Introduction

Numerous studies in the sub-Saharan Africa region have provided useful insights on potential climatic impacts due to changes in the radiative properties of the surface associated with desertification and deforestation (e.g. Charney 1975, Nicholson *et al* 1998, Xue and Shukla 1993, Lare and Nicholson 1994). However, questions still remain over the magnitude and duration of the changes in surface characteristics that are capable of inducing noticeable effects on

climate (Fuller and Ottke 2002). This study seeks to improve our understanding of fire impacts on surface albedo in the northern sub-Saharan Africa (NSSA) region.

Sub-Saharan Africa is one of the most fire-prone regions of the world with most burning occurring during the dry season (e.g. Roberts *et al* 2009). Wildfires in this region are closely related to the seasonal rainfall variability. Most burning north of the equator is observed between November and February, when the Inter-Tropical Convergence Zone (ITCZ) is south of the equator. Then, fire activity drops between March and July due to increasing rainfall associated with the arrival of the ITCZ (Cahoon *et al* 1992). Similarly, south of the equator, most burning is observed between May and October during the dry period (Barbosa *et al* 1999). These fires occur more frequently in the savannas, and

according to Barbosa *et al* (1999), 51% of the African savanna burns every 2 years, while other vegetation types show a lower fire frequency, once or twice every 8 years. The burning frequency is generally higher in the north than south of the equator (Barbosa *et al* 1999, Roberts *et al* 2009).

Wildfires can significantly alter surface albedo and can create a positive radiative forcing by changing the amount of solar radiation absorbed in the climate system (e.g. O'Halloran *et al* 2012, Randerson *et al* 2006). Wildfires cause other effects such as changes in the carbon mass balance in terrestrial ecosystems, as well as the production of carbonaceous aerosols and trace gases that can enhance or offset the effects of changes in albedo (Randerson *et al* 2006, Andersen *et al* 2003). In Africa, wildfires are a key player in terrestrial ecosystems disturbance (e.g. Goldammer and de Ronde 2004). They directly influence the albedo of a surface through a number of short- and long-term effects (e.g. Pinty *et al* 2000, Govaerts *et al* 2002). On shorter timescales, the blackened surface following a fire can lead to some short-lived warming of the surface due to its lower albedo (Govaerts *et al* 2002). The long-term effects of biomass burning on albedo can be related to the widespread replacement of low albedo forests with croplands and grasslands that have higher albedo. So albedo may recover from resprouting vegetation within a few months in a tropical grassland, but require decades in a boreal forest (Randerson *et al* 2006). However, this dependence of albedo recovery on vegetation type is difficult to quantify properly owing to a large spatial and temporal variability due to other factors such as seasonal changes in vegetation cover, rainfall, and intensification of land use as measured by population density (Fuller and Ottke 2002). The complex linkage of surface albedo dynamics with changes in climate and human activities constitutes an important problem that deserves attention.

This study is a part of an interdisciplinary effort investigating the effects of intense biomass burning on the declining regional water resources as exemplified by the drying of Lake Chad (Le Houérou 1996) in a region that comprises a wide range of vegetation and climatic zones over a relatively narrow latitudinal belt (0–20°N). The interdisciplinary study seeks to assess surface, atmospheric and water cycle processes in the region through remote sensing and modelling approaches that integrate research, systems engineering, and applications expertise to best make the connections between various identified processes and phenomena. Such an approach ensures concrete results for societal benefits and climate assessments. Here, we focus on three science questions:

  (i) How does surface albedo change due to biomass burning?
 (ii) How long do these changes in surface albedo persist following fire?
(iii) How might these changes contribute to radiative forcing?

We will address questions (i) and (ii) in this study, while (iii) will be left for future work. The remainder of this paper is organized into three main sections. Section 2 describes the methods used in the analysis of the moderate resolution imaging spectroradiometer (MODIS) albedo time series, albedo gap filling, and determination of albedo change and recovery. Section 3 describes the spatial-temporal extent of vegetation fires in NSSA (cf figure 1), and albedo change and recovery following fire activities for different land cover types in the NSSA region. Section 4 concludes with a summary of the study.

2. Data and methods

2.1. MODIS albedo

Satellites are ideal for providing observations needed for description of surface albedo on a global scale, but we must contend with issues such as uncertainty of the measurements due to atmospheric effects, inadequate sampling (spectral, spatial and temporal), and directionality of these measurements. The global MODIS (Collection 5) albedo product, MCD43A3, (https://lpdaac.usgs.gov/products/modis_products_table/, 1 September 2012) combines measurements from both Terra and Aqua satellites to retrieve directional hemispherical reflectance (black-sky albedo) and bihemispherical reflectance (white-sky albedo) at local solar noon as both spectral (seven narrow spectral bands, MODIS channels 1–7; http://modis.gsfc.nasa.gov/about/specifications.php, 1 September 2012) and three broadband (0.3–0.7 μm, 0.7–5.0 μm, and 0.3–5.0 μm) quantities.

The albedo is derived from the bidirectional reflectance-distribution function (BRDF) model parameters that are retrieved from all high-quality, cloud-free, atmospherically corrected surface reflectance, acquired sequentially over a 16 day period at a spatial resolution of 500 m. The 16 day interval provides an appropriate trade-off between the availability of sufficient angular samples and the temporal stability of the surface (Schaaf *et al* 2002, Wanner *et al* 1997). However, the assumption of stability becomes more tenuous during periods of strong phenological change such as vegetation green-up, senescence, harvesting, or even snowfall or meltdown, when surface characteristics change abruptly. The synergistic use of MODIS observations from both Terra and Aqua offers an opportunity to increase the angular sampling, and helps to improve the coverage and quality of global BRDF and albedo retrievals (Salomon *et al* 2006). Note that Terra has a descending equatorial crossing time of 10:30 a.m., while Aqua has an ascending orbit with a 1:30 p.m. equatorial crossing time. High quality retrievals are obtained during periods of intermittent clear-sky observations by overlapping processing of the data such that retrievals are attempted every 8 days (based on all clear sky observations over the 16 days). However, during long periods of clear sky conditions, the 8 day overlapping introduces an autocorrelation between retrievals, since some of the observations wind up being used in more than one period of retrieval (Schaaf *et al* 2002).

We used high-quality white-sky broadband albedo (0.3–5.0 μm), provided within the MODIS BRDF and albedo quality product (MCD43A2), to assess the impact of biomass burning on surface albedo. The white-sky albedo is derived
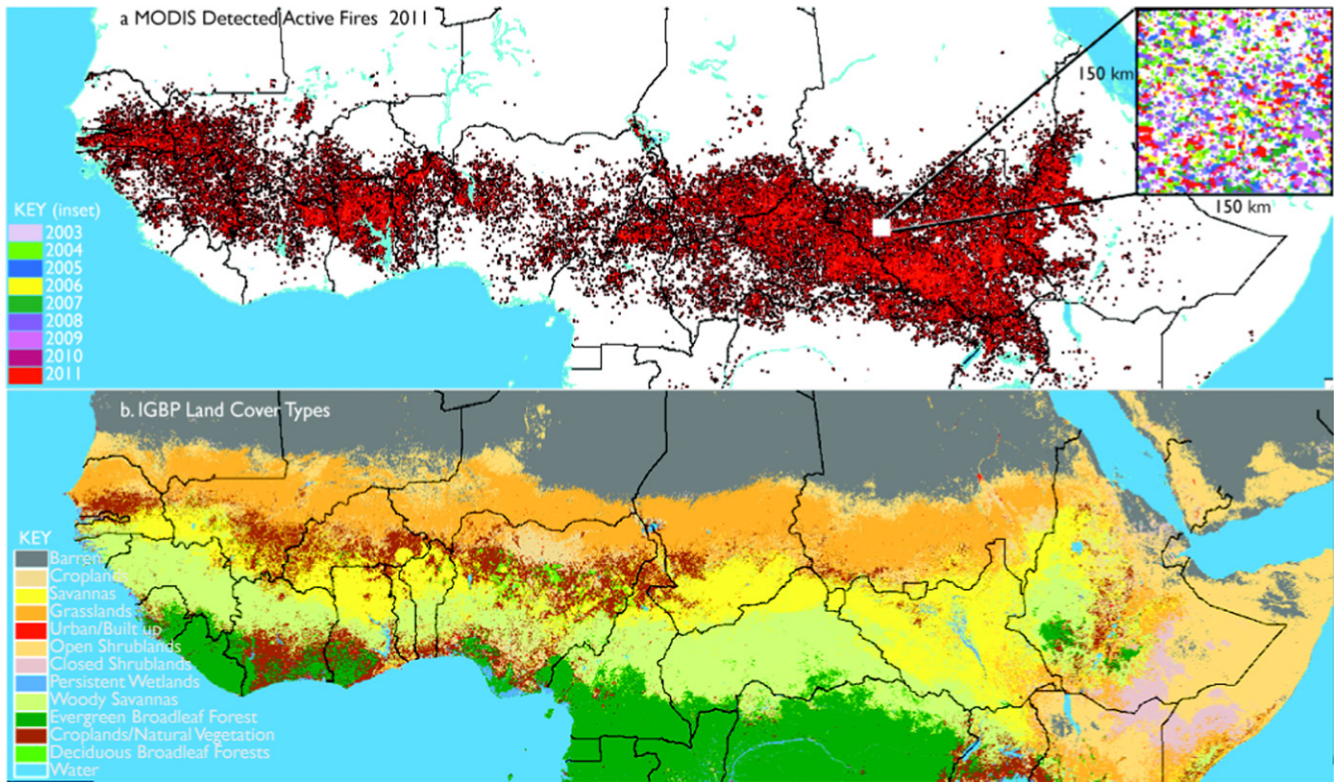
Figure 1. (a) Spatial distribution of MODIS detected fires in 2011. A similar pattern was observed for each year during 2003–11. The inset shows fire distribution for all the years (2003–11) over a small area, 150 km × 150 km in Southern Sudan. Most fires occurred in the savannas and grasslands. (b) Spatial distribution of the main types of land cover in the Northern sub-saharan Africa. Barren or sparsely vegetated lands occupy the largest area (25%), followed by woody savannas and grasslands, each at 15% (cf section 3.1).

from BRDF measurements, integrated over both incoming and outgoing hemispheres, and does not depend on the illumination and atmospheric conditions. Oftentimes, the high quality retrievals contain significant data gaps (Gao *et al* 2008), especially in periods of significant cloud cover, where insufficient angular sampling leads to a magnitude inversion (rely on *a priori* BRDFs based on recent high quality MODIS retrievals at that location as a first guess and adjusting these by the available observations) rather than a full-model inversion (Schaaf *et al* 2002). A full model inversion is attempted only when at least seven cloud-free observations of the surface are available during a 16 day period, and the directional observations adequately sample the view/illumination geometry.

2.2. Gap filling method and validation

As described in section 2.1, MODIS albedo time series contains data gaps where albedo is not retrieved because of problems such as low data quality, persistent or cloud contamination, and poor illumination conditions, which lead to insufficient angular sampling and a lower accuracy on BRDF and albedo. To address the resulting data gap problem, we developed a simple algorithm for producing temporally smoothed and spatially complete MODIS white-sky albedo data set. This gap-filling algorithm first examines each pixel time-series for data gaps and then assigns it one of the five categories determined by the number of consecutive data gaps

k in the time-series ($k = 1$, or 2, or 3, or 4, or $\geqslant 4$ gaps). Note that the largest data gap (four consecutive missing observations) represents a temporal gap of about a month and the albedo is assumed to be stable or changes slowly except during the transition period. For classes with gaps $k = 1, \ldots, 4$, the missing values are determined from equation (1):

$$\alpha_t = \alpha_{t-1} + \left(\frac{\alpha_{t+1} - \alpha_{t-1}}{d_{t+1} - d_{t-1}} \right) (d_t - d_{t-1}), \tag{1}$$

where α_t is the missing albedo value on a Julian day, d_t, α_{t-1} is the last existing albedo value in the time series, and α_{t+1} the first albedo value in the time series after the gap. While a majority of the missing values are determined from equation (1), the method does not work well when there are more than four consecutive missing values in a time series. In this case, an attempt is made to use neighbouring pixels to estimate the missing albedo value within a small window defined by 11 × 11 MODIS 500 m pixels around the missing value, and having the same land cover type as defined by the MODIS Land Cover product (MCD12Q1). If there are no pixels of the same land cover type as the missing value in the selected window, the algorithm progressively increases the search-window size to 31 × 31, or 61 × 61, or 121 × 121, while automatically continuing the search until a suitable albedo match is found. If the algorithm finds no pixels within the maximum search distance (121 × 121 MODIS 500 m pixels), the missing value is replaced by a long-term average albedo

Table 1. Average gap-filling error in albedo for different land cover types in the NSSA.

MODIS Tile: h-20, v-07	$N = 600$ pixels; error (%)			
	1-gap	2-gaps	3-gaps	4-gaps
Barren/sparsely veg.	−0.15	0.02	1.32	0.02
Savanna	−1.73	−2.92	−7.32	−15.5
Woody savanna	−1.93	−5.53	−12.9	−21.13
Grassland	−0.47	−1.22	−1.45	−1.7
Open shrubland	−0.02	0.82	1.37	−0.43
Crop/nat. vegetation	−1.45	−3.6	−8.93	−13.71
Closed shrub	−1.26	−1.28	0.12	−9.44
Cropland	−0.98	−0.45	−5.79	−10.94
Deciduous broadleaf	−2.9	−5.25	−12.19	−17.41

derived from the 2003–11 MODIS albedo of each land-cover type in the entire study region. This approach ensures that every gap is filled with an albedo value that has similar characteristics as the missing pixel and impacted by the same weather systems.

To verify the efficacy of the gap filling algorithm to MODIS measurements, we tested the gap filling method by masking a part of the 'observed' data, which were randomly selected from different land cover types, and applied the gap filling method on these observations and then determined the accuracy of the gap filling method. Table 1 shows average errors (%; (estimated—observed)/observed), where absolute values range from 0.02–2.90% (1-gap), 0.02–5.53% (2-gaps), 0.12–12.90% (3-gaps), and 0.02–21.13% (4-gaps). The errors were small for barren, grasslands and open shrubland, but increase with gap length for savanna, crop/natural vegetation, and deciduous broadleaf forests. The gap-filling method performs well, but generally underestimates the albedo values.

To check the robustness of our gap-filling approach, we applied it to MODIS measurements over a different region in the Southern Great Plains (SGP), Central Facility (36.60°N, 97.48°E), Oklahoma, USA. The SGP was selected because the site has coincident airborne surface reflectance measurements from NASA's Cloud Absorption Radiometer (CAR; Gatebe *et al* 2003, King *et al* 1986). The airborne data were acquired during the 2007 Cloud and Land Surface Interaction Campaign (CLASIC'07) on 24 June 2007. MODIS data cover a period of 32 days, centred around 24 June 2007 (day-of-the-year, DOY, 175). That period was dominated by cloudy skies and heavy rainfall in the region, resulting in a lot of missing albedo values (Román *et al* 2011) that had to be filled to create a good dataset to evaluate the gap filling method. Thus, we used the coincident retrievals from CAR to conduct first-order evaluation of the gap filled approach (cf table 2; figure 2, MODIS albedo2). We also compared our method to the MODIS temporally smoothed and spatially continuous albedo method by Gao *et al* (2008) (cf table 2; figure 2, MODIS albedo1). Note that we used the full expression for all retrievals from aircraft (CAR) and MODIS gap filled approaches (albedo1 and albedo2), as described in Román
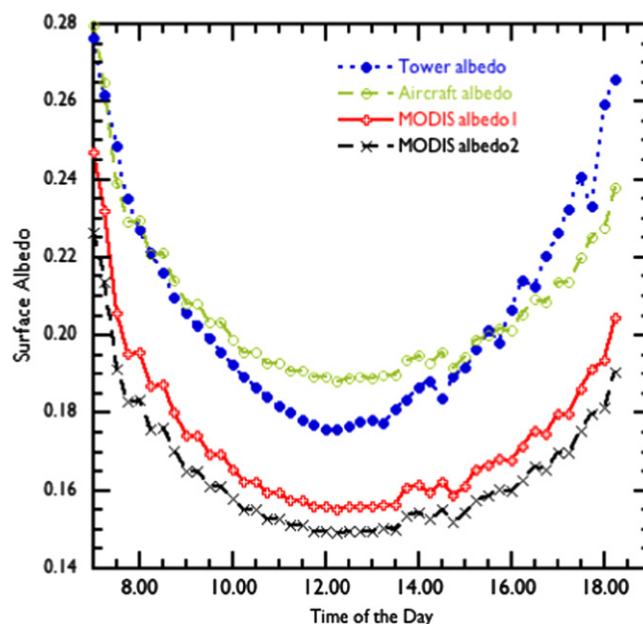

Figure 2. Comparisons between albedos (15 min intervals) derived from airborne CAR, tower-based measurements, and satellite MODIS using two different gap filled approaches over the CART site on 24 June 2007 during CLASIC field campaign. The difference between daily average MODIS and aircraft/tower albedo varies from 15–20% (cf table 2).

et al (2010). Although MODIS albedo values are systematically biased low against aircraft/CAR albedo and tower based albedo by about 15–20%, the two gap-filling methods (albedo1 and albedo2) agree to within 4–5% (cf table 2), but the new approach is simpler and uses mainly the most recent values on either side of the gap and land cover to fill the missing values. On the other hand, MODIS gap filling approach (Gao *et al* 2008) is much more rigorous and normally fit at least 18 months to adequately capture the phenology and bridge a gap. These systematic differences should have little or no impact on the determination of albedo change due to fires.

2.3. Determination of albedo change due to fires

We estimated changes in the albedo after vegetation fires for 11 major land ecosystem types in Africa that were derived from the annual MODIS Land Cover product (MOD12Q), Collection 5 (Friedl *et al* 2010), using the IGBP classification scheme. Barren or sparsely vegetated lands occupy a large area of the study region, 25%, followed by woody savanna, 15%, grassland, 15%, savanna, 11%, open shrubland, 11%, evergreen broadleaf, 10%, cropland or natural vegetation, 8%, closed shrubland, 2%, cropland, 2%, persistent wetland, 0.6%, deciduous broadleaf and others, ∼0.003%. Since most fires (99%) were reported in seven of the land cover classes: savanna (37.7%), woody savanna (48.7%), grasslands (4.8%), cropland or natural vegetation (5.6%), evergreen broadleaf (0.7%), open shrubland (0.7%) and croplands (0.9%), we will focus our analysis on these land cover types.

Table 2. Accuracy and uncertainty values resulting from a 32 day comparison between airborne (CAR) and satellite-derived (MODIS) albedos using two different gap-filling approaches.

a. All Days	10°≤SZA ≤45° (n = 289)			45°≤SZA ≤75° (n = 193)		
DOY 159–190	Aircraft/(CAR)	MODIS/albedo1	MODIS/albedo2	Aircraft/(CAR)	MODIS/albedo1	MODIS/albedo2
Accuracy	0.0042	−0.0286	−0.0333	−0.0096	−0.0495	−0.0570
Uncertainty	0.0082	0.0296	0.0341	0.0184	0.0526	0.0589

The albedo change caused by biomass burning was determined at the pixel level for each land cover type using the 2003–11 MODIS albedo data record in the entire NSSA region on a monthly basis. A pixel was considered burned when an active fire was reported in the MODIS Level-3, 8 day daily active fire product (MOD14A2) at the 1 km grid cell, assuming all the fire detection confidence levels (low-confidence fire, nominal-confidence fire, or high-confidence fire). The decision to consider fires in all confidence classes was meant to ensure that we have sufficient statistical samples for the less fire-affected land cover types, especially during the non-fire season months. Overall, the low-confidence cases accounted for <5% of all the MODIS fires detected during 2003–11 for most of the land cover types, and therefore, had little influence on the albedo perturbation estimates. The study focuses more on the albedo changes during the fire season and assumes that all 4×500 m MODIS albedo pixels burn for each 1 km active fire pixel detection. Here, we define the average albedo change Δ_c due to vegetation fires for a particular land cover type c as:

$$\Delta_c = \frac{1}{N} \sum (\alpha_{\text{post}} - \alpha_{\text{pre}}), \qquad (2)$$

where, α_{pre} is the albedo of a pixel before fire was observed by MODIS and α_{post} is the albedo of the burned pixel, 24 days after fire was reported. Note that the 24 days were chosen to minimize autocorrelation caused by the 16 day data processing interval for the MODIS albedo product, which is produced every 8 days.

2.4. Estimation of albedo recovery

We used post-fire surface changes to describe post-fire recovery in different ecosystems. This was deduced from the time it took albedo to return to within 5% of its pre-fire value based on the post-fire albedo time series. This approach is illustrated in figure 3, where a time series of albedo of a burnt pixel is compared to the albedo of a control pixel. The control was selected from neighbouring pixels of the same land cover type, which showed similar albedo characteristic patterns over an extended period of time (at least 2 years prior to the fire event). Note that the interval between data points in figure 3(a) is 8 days. Figure 3(b) shows the same data, but zooming into the fire period in order to show details of the albedo recovery after the fires. Our algorithm computed the recovery period as the amount of time it took the burnt pixel to recover to within 5% of the pre-fire albedo. The 5% threshold was arbitrary, but it helped to deal with cases where

a sudden increase occurred as the albedo approached the pre-fire value. For both pixels, the pre-fire albedo values exhibit a seasonal trend consistent with the vegetation phenology changes from senescence to green-up. The corresponding post-fire albedo values follow a similar trend, but the control pixel shows consistently lower values after the fire is detected (gray-shaded region in figures 3(a) and (b)). Since the points represent albedo every eight days, the recovery period in this case takes 288 days or less than a year. Figure 3(c) shows a plot of albedo time series of both burned and unburned savanna pixels over a longer period (8 years) to further illustrate how this approach works. In this case fire was detected on 26 June 2006 and the recovery took about 1 year and a 3 months, and so the albedo had recovered by 8 October 2007.

3. Results

3.1. Spatial-temporal extent of vegetation fires in the NSSA

In the NSSA region, most fires are detected south of the Sahara desert almost across the whole region from west to east (figure 1(a)). Some areas such as Southern Sudan appear to be more fire-prone than others, as nearly every square km of land seems to have been affected by fire at least once between 2003 and 2011 (cf figure 1(a): inset). During that 9 year period, with approximately two overpasses by Terra every 24 h (once during the day and once at night), the total MODIS active fire-pixel count at 1 km resolution in the entire NSSA region is about 2.2 million, with an annual average of about 11% of the total fire count. Indeed, this confirms that Africa has one of the highest frequencies of fire occurrence of fire per land area than any other continent (cf Ichoku *et al* 2008). The occurrence of wildfires is more frequent in the savannas (woody savanna and savanna), which account for >86% of the total MODIS fire count between 2003 and 2011 (table 4, column 2 and figure 1(b)). Hence, the spatial-temporal extent of vegetation fires in sub-Saharan Africa is widespread, and the disturbance rates from year to year remain uniform based on MODIS fire count between 2003 and 2011. We note that these fire statistics are likely an underestimate of the actual fire activity, since smaller and cooler fires are probably missed due to the relatively high thresholds used in the MODIS global fire detection algorithm (Giglio *et al* 2003, Justice *et al* 2002).

Because the frequency with which fire returns to a given ecosystem is an important component of its fire regime and influences albedo perturbation, we also determined the ratio
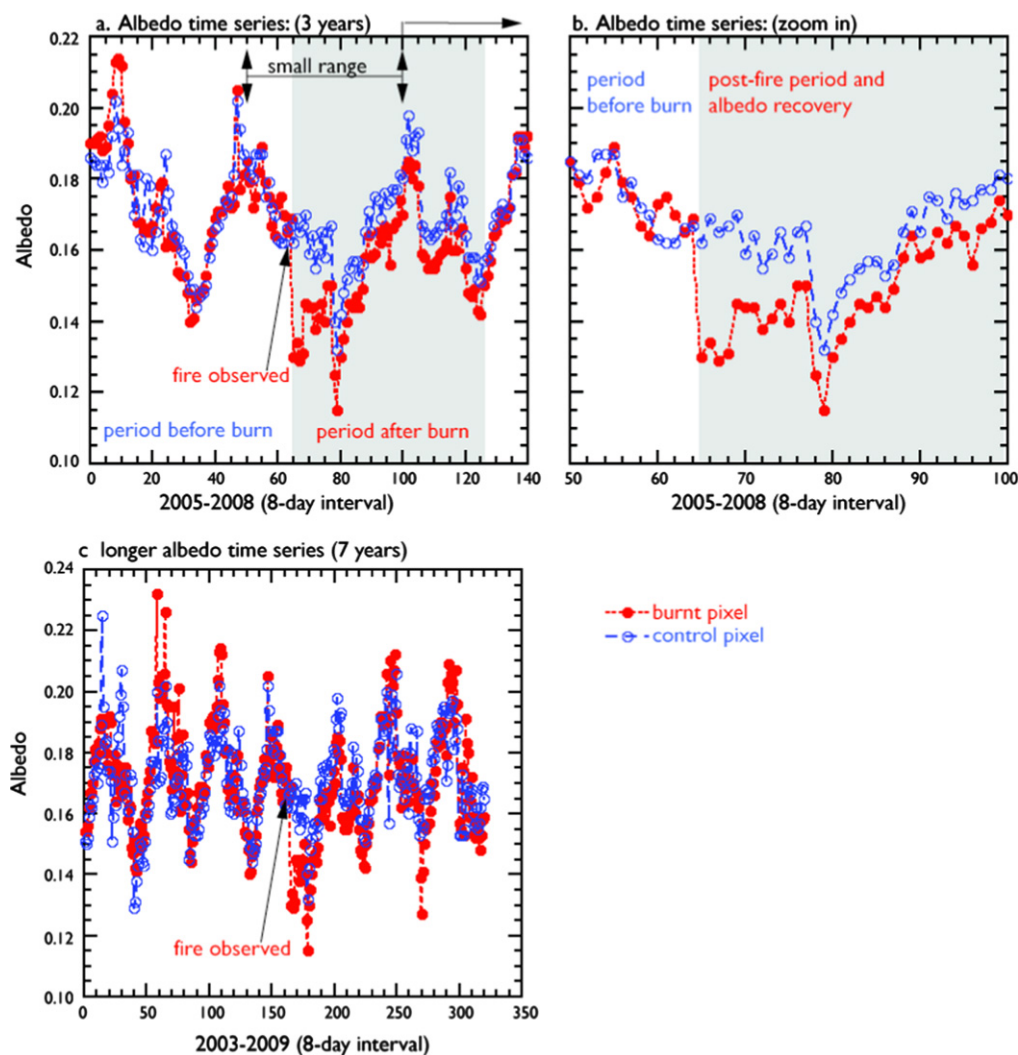
Figure 3. (a) An example of albedo time series of a burned savanna pixel (red line) and its corresponding control pixel (blue line) beginning 10 Feb 2005 to 2 Feb 2008. The gray-shaded area represents mostly the post-fire period. (b) Same as (a), but zooming into the post-fire period. The control pixel mimics the burned pixel without fire. Fire was detected on 26 June 2006 and its effect on albedo lasted for about 288 days. (c). Time series to show the pattern over a longer period. In this case fire was detected on 26 June 2006. Albedo was fully recovered by December 2007.

of the number of pixels that burned at successive intervals (1–8 years; starting with pixels that burned in 2003) to the total number of pixels that burned in 2003 in each land cover type. Figure 4(a) shows results of this analysis, where only about 10% of the savanna pixels that burned in 2003 burned again after 1 year and the number decreases almost linearly in subsequent years. A total of 47% pixels burned again by 2011. The evergreen broadleaf shows a different pattern, where there is a peak between the third and fourth year, and a second peak seems to be forming after the eighth year. A total of 15% of the evergreen broad leaf pixels that burned in 2003 had burned again by 2011. Figure 4(b) shows the fire count ratios for the other land cover types. Note that the total numbers of pixels that burned again differs in each case in 9 years (woody savanna, 40%; grasslands, 35%; open shrubland, 28%; cropland, 34%; and cropland or natural vegetation, 27%). In the following sections, we are going to look at the results of albedo perturbation and the albedo recovery.

3.2. Albedo perturbation caused by biomass burning

It is important to critically examine the impacts of fire-induced albedo perturbation and recovery. Table 3 shows the average albedo values of different land cover types before fire was reported. We averaged the pre-fire values in each pixel in a given month for the period 2003–11. Table 4 shows the albedo change as derived from equation (3) for each of the land cover types. The standard deviation in each case represents the temporal and spatial variability of the albedo or albedo perturbation. The albedo change caused by fires varies by ecosystem type as depicted in figure 5 and table 4. Some ecosystems show large values of the standard deviation partly because of post-fire changes in surface albedo associated with dissipation of charcoal and ash, and vegetation regrowth over the 24 days period used to calculate monthly post-fire albedo change (cf Amiro *et al* 2006, Jin and Roy 2005). All land cover types show a decrease in albedo after fires, except for croplands, which show an increase after fire probably related
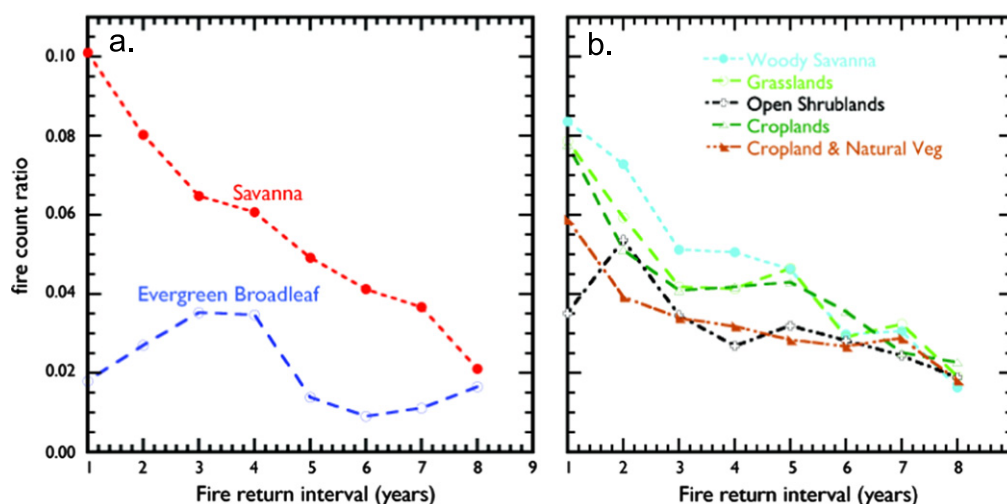
Figure 4. Ratio of the number pixels that burned at successive intervals (1–8 years; given that the pixel burned in 2003) to the total number of pixels that had burned in 2003 for different land cover types. For savanna, ⩽10% of the pixels that burned in 2003 burned again in 2004 and a total of 47% of the pixels burned at least twice within a period of 9 years.

to the exposure of the underlying soils with higher albedo (Hoffa *et al* 1999). For the majority of the land-cover types, the albedo darkening is probably related to the deposition of charcoal and ash, or vegetation growth. While fires reduce or darken the surface albedo as observed during the fire season (figure 5), there are cases where the monthly albedo perturbations show an increase especially during the northern hemisphere summer months (cf table 4). Higher spatio-temporal variability in the albedo during these months could account for greater uncertainty in characterizing the undisturbed albedo. Quantifying the albedo perturbation during these months is further hampered by the relatively few fire events.

The satellite-derived albedo perturbations in this study are several orders of magnitude smaller compared to points or tower measurements immediately following a fire. For example, Beringer *et al* (2003) reported a drop of about 42% immediately following a fire. Large differences are to be expected for comparisons of satellite data with the point or tower measurements owing to the greater than 1 km scale of the satellite footprint, which in many cases may integrate signal from both burned and unburned areas in different proportions within each pixel. Jin and Roy (2005) report albedo changes up to a factor of 10 larger than the averages reported in table 4 in a study of satellite data for Australian savannas. This difference might be attributable to limited geographical coverage (Africa, 0–20°N versus Australia north of 26.5°S) and/or the large statistics considered in our study (9 years versus 1 year). Govaerts *et al* (2002) estimate albedo changes from all daylight Meteosat-5 data acquired during January and December in 1996 over sub-Saharan Africa range from 5% to 8% of the unburned albedo. The corresponding values for savannas surfaces in table 4 are slightly smaller than the lower end of the Govaerts *et al* (2002) range. We note that the derived surface albedo perturbation in the Govaerts *et al* (2002) is the hemispherical integration of the BRF for a given position of the Sun fixed at 30°, estimated

within the Meteosat radiometer visible (VIS) band running approximately from 0.4 μm up to 1.1 μm. Therefore, these differences between the two studies are to be expected.

3.3. Post-fire albedo recovery

The post-fire albedo recovery is important for the radiative forcing estimates and for modeling post-fire albedo dynamics (both seasonal or annual). Table 5 and figure 6 summarize the post-fire albedo recovery in terms of percentage of pixels that recover to pre-fire values for burn events that took place in 2003 tracked cumulatively at 3 month intervals over a period of 7 years for the land cover types investigated. At each step, we normalized by the total number of tracked pixels in their respective land cover types. The albedo recovery after fires progresses rapidly within the first year, with the savannas leading in recovery rate (>77%), and the evergreen broad leaf showing the least recovery (58%). By the end of the second year after fires, over 80% of the burnt pixels for all the biomes recover to their pre-fire albedo. For the savannas, where 86% of burning takes place, the recovery of the burnt pixels exceeds 99% after 5 years. The persistence of surface albedo darkening (or brightening, where applicable) is limited to about 6–7 years, when at least 99% of the burnt pixels recover to their pre-fire albedo for all land cover types. A very basic fitting of the data reveals that the percentage of pixels that recover to their pre-fire albedo values can be described by a simple exponential function:

$$R_t^c = ae^{-1/t^2}, \tag{3}$$

where, R_t^c is the % albedo recovery after t years for any land cover type c, and 'a' is a constant (~50). This simple function explains the observed percentage of pixels that recover to their pre-fire albedo values for a particular land cover type (e.g. savanna, woody savanna, cropland, cropland or natural vegetation, and open shrublands), where the function predicts a minimum recovery of about 50% within the first 3 months

8

Table 3. Average monthly albedo of pixel from MODIS (2003–11) before fire was reported.

Land cover	Jan	Feb	Mar	April	May	June	July	Aug	Sept	Oct	Nov	Dec
Savanna	0.135 ± 0.004	0.147 ± 0.002	0.159 ± 0.002	0.160 ± 0.005	0.162 ± 0.005	0.158 ± 0.005	0.151 ± 0.013	0.143 ± 0.019	0.135 ± 0.014	0.147 ± 0.003	0.130 ± 0.003	0.130 ± 0.002
Woody savanna	0.128 ± 0.004	0.137 ± 0.002	0.148 ± 0.003	0.151 ± 0.005	0.155 ± 0.005	0.157 ± 0.007	0.145 ± 0.014	0.147 ± 0.019	0.137 ± 0.009	0.144 ± 0.002	0.130 ± 0.002	0.126 ± 0.003
Evergreen broadleaf	0.123 ± 0.003	0.127 ± 0.002	0.140 ± 0.006	0.140 ± 0.005	0.138 ± 0.005	0.148 ± 0.008	0.140 ± 0.014	0.138 ± 0.009	0.140 ± 0.017	0.130 ± 0.014	0.130 ± 0.007	0.120 ± 0.006
Grassland	0.155 ± 0.007	0.165 ± 0.004	0.175 ± 0.004	0.180 ± 0.006	0.187 ± 0.012	0.189 ± 0.012	0.166 ± 0.015	0.158 ± 0.012	0.155 ± 0.017	0.161 ± 0.006	0.145 ± 0.003	0.151 ± 0.004
Open shrubland	0.167 ± 0.006	0.184 ± 0.006	0.195 ± 0.015	0.193 ± 0.011	0.201 ± 0.004	0.209 ± 0.016	0.219 ± 0.032	0.228 ± 0.054	0.183 ± 0.022	0.164 ± 0.009	0.155 ± 0.008	0.164 ± 0.007
Crop/nat. vegetation	0.155 ± 0.003	0.162 ± 0.003	0.171 ± 0.003	0.176 ± 0.007	0.178 ± 0.007	0.174 ± 0.006	0.157 ± 0.014	0.161 ± 0.017	0.152 ± 0.011	0.157 ± 0.003	0.151 ± 0.004	0.155 ± 0.003
Cropland	0.155 ± 0.004	0.164 ± 0.006	0.170 ± 0.004	0.172 ± 0.004	0.167 ± 0.006	0.170 ± 0.015	0.157 ± 0.014	0.144 ± 0.017	0.146 ± 0.018	0.160 ± 0.008	0.148 ± 0.006	0.152 ± 0.004

Table 4. Fire frequency and albedo change due fires from MODIS (2003–11) for different land cover types in the NSSA.

|	Fire count (%)	Albedo change ($\times 10^{-3}$)											
		Jan	Feb	Mar	Apr	May	Jun	Jul	Aug	Sep	Oct	Nov	Dec
Savanna	37.73	−2.0 ± 3.5	−3.7 ± 4.3	0.7 ± 5.0	1.3 ± 3.5	1.7 ± 3.5	5.1 ± 4.8	1.2 ± 8.1	−0.5 ± 9.8	0.5 ± 6.0	4.2 ± 4.8	0.1 ± 2.6	−3.1 ± 3.4
Woody Savanna	48.69	−1.1 ± 3.7	−3.0 ± 4.0	−0.9 ± 3.4	−0.1 ± 2.5	0.2 ± 2.5	1.9 ± 5.1	3.8 ± 15.0	−0.3 ± 10.4	3.2 ± 7.4	3.3 ± 3.7	2.4 ± 2.8	−2.1 ± 3.2
Evergreen broadleaf	0.71	2.0 ± 3.4	−4.9 ± 7.2	0.4 ± 6.1	−1.4 ± 5.9	−1.2 ± 8.7	−2.3 ± 12.0	7.5 ± 18.9	−0.7 ± 14.5	5.9 ± 16.0	−0.2 ± 15.0	2.1 ± 4.9	−2.4 ± 4.3
Grassland	4.78	−0.8 ± 2.8	−3.0 ± 4.1	−0.5 ± 3.8	1.9 ± 3.9	−2.3 ± 3.7	3.7 ± 6.9	2.4 ± 14.3	4.4 ± 12.5	−1.4 ± 4.9	−0.8 ± 3.2	0.1 ± 3.4	−0.6 ± 3.7
Open shrubland	0.67	0.0 ± 3.1	−2.0 ± 3.8	−0.3 ± 4.5	1.2 ± 5.2	−0.4 ± 3.5	7.6 ± 7.1	9.6 ± 10.4	−6.3 ± 12.3	−1.6 ± 6.3	−0.7 ± 2.6	1.5 ± 3.2	−1.5 ± 3.2
Crop/nat. vegetation	5.59	−0.2 ± 2.4	−2.6 ± 3.0	0.5 ± 4.6	0.5 ± 3.0	−0.6 ± 4.0	1.6 ± 7.3	2.1 ± 14.1	−1.8 ± 15.2	0.2 ± 6.5	−0.5 ± 1.6	1.1 ± 3.3	−0.7 ± 2.8
Cropland	0.89	1.1 ± 3.8	−3.2 ± 3.7	1.0 ± 6.0	2.0 ± 4.5	−3.0 ± 5.2	0.5 ± 7.6	−1.8 ± 13.0	−1.9 ± 16.7	0.6 ± 6.0	−0.3 ± 3.3	3.1 ± 5.0	1.0 ± 2.3
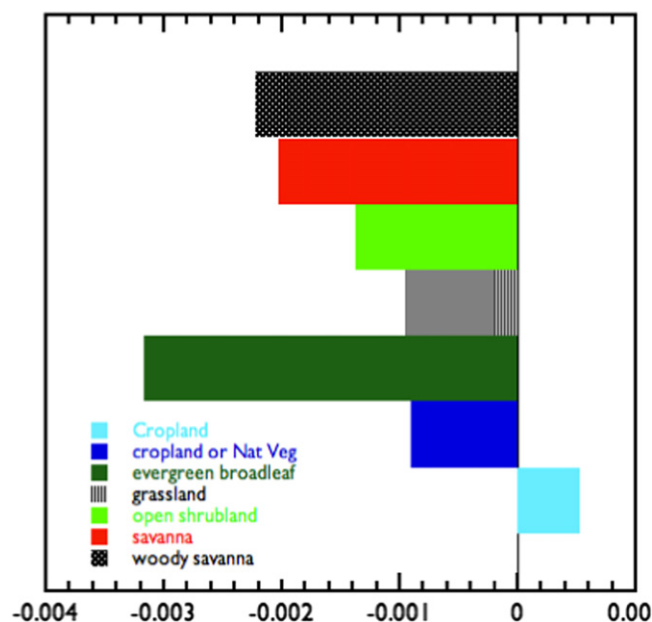
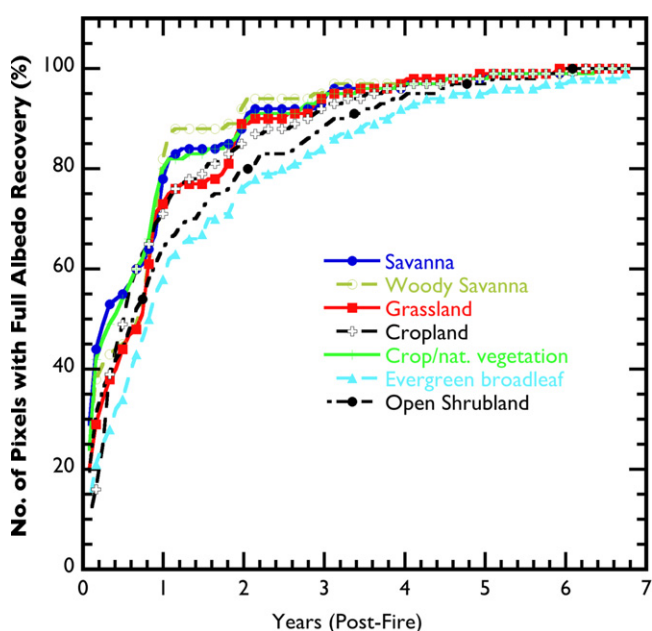**Figure 5.** Albedo perturbation during the fire season (November–March).

Figure 6. Percentage of pixels burned in 2003 that has recovered by each subsequent year tracked over a period of 7 years for different land cover types in northern sub-Saharan Africa. Points are plotted every 90 days.

after fire. However, it overestimates the recovery of the other land cover types (e.g. evergreen broad leaf) by about 30% within the first 3 months after the fire. It is very clear from this analysis that the percentage of pixels that recover to their pre-fire albedo values, as determined from satellite data, provides another perspective on how fast the albedo recovers over various land-cover types in the NSSA region. However, in order to apply these results to radiative forcing and modeling studies of post-fire albedo dynamics, a relationship with actual albedo recovery (both seasonally and annually) has to

be established and validated. That task is beyond the scope of the current study, but need to be developed in future.

4. Summary and conclusions

The extent of wildfires in Africa can be seen clearly from a map of active fire detected by satellite sensors such as the MODIS aboard Terra and Aqua at their times of overpass under relatively cloud-free conditions. We found that the spatial-temporal extent of vegetation fires in sub-Saharan Africa is widespread, and the disturbance rates from year to year remain uniform based on MODIS fire count between 2003 and 2011. We also found that only a small fraction of the pixels ($\leqslant$10%) burn twice in two successive years and $\leqslant$47% in 9 years.

We estimated the change of surface albedo due to fires over different land cover types in the NSSA using long MODIS time series for the period of 2003–11. We found a decrease in albedo over most land cover types due to fires (e.g. woody savanna ($-0.002\,02 \pm 0.000\,03$) and savanna ($-0.002\,22 \pm 0.000\,03$), which accounted for >86% of the total MODIS fire count between 2003 and 2011. Evergreen broadleaf had a larger reduction ($-0.003\,17 \pm 0.000\,03$) than the savanna, but accounted for only about 0.7% of the total fire count. The observed monthly albedo perturbation in each month for various biomes in NSSA is variable, while the largest values were observed in July, probably caused by uncertainties due to rapidly changing albedo associated with the peak growing season. During the fire season the albedo decrease is correlated with peak fire count of most of the investigated land cover types (e.g. savanna), possibly related to post-fire albedo darkening due to dissipation of charcoal and ash, or vegetation regrowth. However, for very few land cover types (e.g. croplands), there is albedo increase that is correlated with peak fire count, probably related to the exposure of the underlying soils with higher albedo.

The study demonstrates a simple method for deriving the trajectories of post-fire albedo dynamics from satellite data that is consistent and widely available. The percentage of pixels that recover to their pre-fire albedo values provide some insights on how fast the albedo recovers over various land-cover in the NSSA region. The persistence of surface albedo darkening (or brightening, where applicable) is limited to about 6–7 years. The albedo recovery after fires can be described by a simple exponential function, regardless of vegetation type.

Our results can provide critical information for deriving necessary input to various models used in the different aspects of the broader interdisciplinary research in determining the regional atmospheric heating rates due to biomass burning and effects on the radiative forcing and feedbacks in the NSSA region. They can also be useful in the land-surface models to determine the effects of albedo changes due to fires on soil moisture budget, evapotranspiration, infiltration, and runoff, all of which govern the land-surface component of the water cycle. Our surface albedo change results can be ingested in atmospheric models, where they can serve as part

Table 5. Post-fire albedo recovery after every three months.

	No of burnt pixels with full-albedo recovery (%)					
Yrs	Savanna	Woody savanna	Grassland	Cropland	Cropland nat. veg	Evergreenbroadleaf	Open Shrubland
0.25	49.25	41.18	34.47	24.58	45.94	25.46	35.92
0.49	55.47	44.61	43.71	49.49	53.61	33.72	43.69
0.74	60.94	53.06	51.35	62.63	62.12	45.87	54.13
0.99	77.93	81.77	73.02	71.38	79.79	58.26	64.32
1.23	83.71	88.01	76.87	77.10	82.39	64.91	69.17
1.48	84.13	88.21	77.45	79.12	83.17	67.20	71.60
1.73	84.64	88.49	78.91	82.32	84.15	70.87	75.49
1.97	87.99	91.99	88.73	85.35	88.17	75.92	79.61
2.22	92.00	94.17	90.25	87.21	91.10	78.90	82.52
2.47	92.18	94.21	90.47	87.88	91.16	79.59	83.01
2.71	92.31	94.33	90.91	89.56	91.62	81.42	84.71
2.96	93.21	95.49	94.11	91.58	94.28	84.40	87.62
3.21	95.75	96.83	94.98	93.43	95.19	86.70	89.81
3.45	95.88	96.90	95.56	94.44	95.52	88.07	91.26
3.70	95.93	96.99	95.78	95.45	95.78	89.91	92.96
3.95	96.20	97.31	97.16	96.46	96.56	91.51	94.42
4.19	97.71	98.26	97.96	97.14	97.21	93.35	95.15
4.44	97.76	98.30	98.11	97.31	97.40	94.04	95.87
4.68	97.83	98.34	98.11	97.98	97.60	94.95	96.84
4.93	98.06	98.55	98.55	98.15	98.05	95.18	97.09
5.18	99.35	99.30	99.20	98.65	98.64	96.10	98.06
5.42	99.39	99.32	99.27	98.99	98.64	96.33	98.30
5.67	99.41	99.36	99.27	98.99	98.64	96.33	98.30
5.92	99.50	99.47	99.71	99.16	98.77	96.79	99.03
6.16	99.87	99.90	99.93	99.66	99.48	97.71	99.76
6.41	99.88	99.91	100.00	99.83	99.55	97.94	100.00
6.66	99.88	99.91	100.00	100.00	99.94	97.94	100.00

of the essential input parameters based upon which radiative energy budget estimates are made, both at the surface and at the top of the atmosphere. As such, these models can better characterize the effects of change in surface albedo due to fires on the atmospheric heating rates of the black carbon aerosols emitted by fires, which can affect the atmospheric component of the water cycle through the interaction of radiation with surface albedo and the aerosol indirect radiative effects on clouds. Furthermore, information on the spatial and temporal dynamics of the post-fire albedo recovery will be important in modelling the medium- to long-term climate impacts of fires in the NSSA region.

Acknowledgements

References

Amiro B D *et al* 2006 The effect of post-fire stand age on the boreal forest energy balance *Agric. Forest Meteorol.* **140** 41–50

Andersen A N, Cook G D and Williams R J 2003 *Fire in Tropical Savannas: The Kapalga Experiment* (New York: Springer)

Barbosa P M, Stroppiana D and Gregoire J-M 1999 An assessment of vegetation fire in Africa (1981–1991): burned areas, burned biomass, and atmospheric emissions *Glob, Biogeochem. Cycles* **13** 933–50

Beringer J, Hutley L B, Tapper N J, Coutts A, Kerley A and Grady A P O 2003 Fire impacts on surface heat, moisture and carbon fluxes from a tropical savanna in northern Australia *Int. J. Wildland Fire* **12** 333–40

Cahoon D R Jr, Stocks B J, Levine J S, Cofer W R 3rd and O'Neill C P 1992 Seasonal distribution of African savanna fires *Nature* **359** 812–5

Charney J G 1975 Dynamics of deserts and drought in the Sahel *Q. J. R. Meteorol. Soc.* **101** 193–202

Friedl M A, Sulla-Menashe D, Tan B, Schneider A, Ramankutty N, Sibley A and Huang X 2010 MODIS collection 5 global land cover: algorithm refinements and characterization of new datasets *Remote Sens. Environ.* **114** 168–82

Fuller O D and Ottke C 2002 Land cover, rainfall and land-surface albedo in West Africa *Clim. Change* **54** 181–204

Goldammer J G and de Ronde C 2004 *Wildland Fire Management Handbook for Sub-Sahara Africa* (Freiburg, Cape Town: Global Fire Monitoring Center and Oneworld Books) p 432

Gao F, Morisette J T, Wolfe R E, Ederer G, Pedelty J, Masuoka E, Myneni R, Tan B and Nightingale J 2008 An algorithm to

produce temporally and spatially continuous MODIS-LAI time series *IEEE Geosci. Remote Sens. Lett.* **5** 60–4

Gatebe C K, King M D, Platnick S, Arnold G T, Vermote E F and Schmid B 2003 Airborne spectral measurements of surface-atmosphere anisotropy for several surfaces and ecosystems over southern Africa *J. Geophys. Res.* **108** 8489

Giglio L, Descloitres J, Justice C O and Kaufman Y 2003 An enhanced contextual fire detection algorithm for MODIS *Remote Sens. Environ.* **87** 273–82

Govaerts Y M, Pereira J M, Pinty B and Mota B 2002 Impact of fires on surface albedo dynamics over the African continent *J. Geophys. Res.* **107** (D22, 4629)

Hoffa E A, Ward D E, Hao W M, Susott R A and Wakimoto R H 1999 Seasonality of carbon emissions from biomass burning in a Zambian savanna *J. Geophys. Res.* **104** 13841–53

Ichoku C, Giglio L, Wooster M J and Remer L A 2008 Global characterization of biomass-burning patterns using satellite measurements of radiative energy *Remote Sens. Environ.* **112** 2950–62

Jin Y and Roy D P 2005 Fire-induced albedo change and its radiative forcing at the surface in northern Australia *Geophys. Res. Lett.* **32** L13401

Justice C O, Giglio L, Korontzi S, Owens J, Morisette J, Roy D, Descloitres J, Alleaume S, Petitcolin F and Kaufman Y 2002 The MODIS fire products *Remote Sens. Environ.* **83** 244–62

King M D, Strange M G, Leone P and Blaine L R 1986 Multiwavelength scanning radiometer for airborne measurements of scattered radiation within clouds *J. Atmos. Ocean Technol.* **3** 513–22

Lare A R and Nicholson S E 1994 Contrasting conditions of surface water balance in wet years and dry years as a possible land surface-atmosphere feedback mechanism in the West African Sahel *J. Clim.* **7** 653–68

Le Houérou H N 1996 Climate change, drought and desertification: review *J. Arid Environ.* **34** 133–85

Nicholson S E, Tucker C J and Ba M B 1998 Desertification, drought, and surface vegetation: an example from the West African Sahel *Bull. Am. Meteorol. Soc.* **79** 815–29

O'Halloran T L *et al* 2012 Radiative forcing of natural forest disturbances *Glob. Change Biol.* **18** 555–65

Pinty B, Verstraete M M, Gobron N, Govaerts Y and Roveda F 2000 Do human-induced fires affect the earth surface reflectance at continental scales? *EOS Trans. Am. Geophys. Union* **81** 381–9

Randerson J T *et al* 2006 The impact of boreal forest fire on climate warming *Science* **314** 1130–2

Roberts G, Wooster M J and Lagoudakis E 2009 Annual and diurnal African biomass burning temporal dynamics *Biogeosciences* **6** 849–66

Román M O, Gatebe C K, Schaaf C, Poudyal R, Wang Z and King M D 2011 Variability in surface BRDF at different spatial scales (30 m–500 m) over a mixed agricultural landscape as retrieved from airborne and satellite spectral measurements *Remote Sens. Environ.* **115** 2184–203

Román M O, Schaaf C B, Lewis P, Gao F, Anderson G P, Privette J L, Strahler A H, Woodcock C E and Barnsley M 2010 Assessing the coupling between surface albedo derived from MODIS and the fraction of diffuse skylight over spatially-characterized landscapes *Remote Sens. Environ.* **114** 738–60

Salomon J, Schaaf C B, Strahler A H, Gao F and Jin Y 2006 Validation of the MODIS bidirectional reflectance distribution function and albedo retrievals using combined observations from the aqua and terra platforms *IEEE Trans. Geosci. Remote Sens.* **44** 1555–65

Schaaf C B *et al* 2002 First operational BRDF, albedo and aadir reflectance products from MODIS *Remote Sens. Environ.* **83** 135–48

Wanner W, Strahler A H, Hu B, Lewis P, Muller J-P, Li X, Schaaf C L B and Barnsley M J 1997 Global retrieval of bidirectional reflectance and albedo over land from EOS MODIS and MISR data: theory and algorithm *J. Geophys. Res.* **102** 17143–62

Xue Y and Shukla J 1993 The Influence of land surface properties on Sahel climate: part I, desertification *J. Clim.* **6** 2232–45